

Article

Prediction of Lithium-Ion Battery Health Using GRU-BPP

Sahar Qaadan ^{1,2} , Aiman Alshare ^{3,*} , Alexander Popp ²  and Benedikt Schmuelling ² 

¹ Mechatronics Engineering, German Jordanian University, Madaba Street, Amman 11180, Jordan; sahar.qadan@gju.edu.jo

² Institute of Electric Mobility and Energy Storage Systems, University of Wuppertal, Rainer-Gruenter-Str. 21, 42119 Wuppertal, Germany; apopp@uni-wuppertal.de (A.P.); schmuelling@uni-wuppertal.de (B.S.)

³ Mechanical and Maintenance Engineering, German Jordanian University, Madaba Street, Amman 11180, Jordan

* Correspondence: aiman.share@gju.edu.jo

Abstract: Accurate prediction of lithium-ion batteries' (LIBs) state-of-health (SOH) is crucial for the safety and maintenance of LIB-powered systems. This study addresses the variability in degradation trajectories by applying gated recurrent unit (GRU) networks alongside principal component analysis (PCA), Granger causality, and K-means clustering to analyze the relationships between operating conditions—such as temperature and load profiles—and battery performance degradation. This paper uses a publicly accessible dataset derived by aging three prismatic LIB cells under a realistic forklift operation profile. First, we identify the features that are relevant to driving variance, then we employ the winning algorithm of K-means clustering for the classification of operational states. Granger causality later investigates the inter-group relationships. Our GRU-BPP model achieves an RMSE value of 0.167 and an MAE of 0.129 for the reference performance testing (RPT) dataset and an RMSE of 0.032 with an MAE of 0.025 for the aging dataset, thus outperformed benchmark methods such as GRU, LME, and XGBoost. These results further enhance the predictiveness and robustness of this approach and yield a holistic solution to the conventional challenges in battery management and their remaining useful life (RUL) predictions.



Citation: Qaadan, S.; Alshare, A.; Popp, A.; Schmuelling, B. Prediction of Lithium-Ion Battery Health Using GRU-BPP. *Batteries* **2024**, *10*, 399. <https://doi.org/10.3390/batteries10110399>

Academic Editor: Rodolfo Dufo-López

Received: 12 October 2024

Revised: 31 October 2024

Accepted: 4 November 2024

Published: 8 November 2024



Copyright: © 2024 by the authors. Licensee MDPI, Basel, Switzerland. This article is an open access article distributed under the terms and conditions of the Creative Commons Attribution (CC BY) license (<https://creativecommons.org/licenses/by/4.0/>).

1. Introduction

Electric vehicles and portable electronics have rapidly developed a demand for efficient and reliable lithium-ion batteries (LIBs) in the market. Longevity, durability, and performance are greatly important for customer satisfaction in LIBs and technological development. Accurate estimation of a battery's SOH is crucial for optimizing the battery usage and preventing sudden failures, which have great economic consequences and safety risks [1,2].

Model-based methods of SOH and RUL estimation solely depend on the physical and chemical nature of the battery for correct estimation. Most of these methods develop mathematical models for describing the activities of the battery in working and weighting conditions. For instance, Baghdadi et al. [3] developed a semi-empirical model based on Dakin's degradation approach to assessing lithium-ion battery cell life loss under various operating conditions. Among these factors, temperature, SOC, and current magnitude are the most influential degradation factors. The logarithms of capacity fade and increase in internal resistance, evolving linearly with time, and this forms a solid basis for predicting battery aging. Zhang et al. [4] integrated a thermal dynamics model for RUL estimation, combining temperature and state of charge to predict battery aging more effectively. Xu et al. [5] developed a stochastic deterioration rate model based on the Wiener process

and the Arrhenius temperature model. This model improves the accuracy of the deterioration predictions by accounting for fluctuating temperature conditions at various times and introducing a stochastic variation of a battery's aging processes.

Dong et al. [6] discussed a physics-based aging model in which the solid electrolyte interphase (SEI) layer's growth and creation is the main aging mechanism. This model predicts lithium-ion battery capacity fade by combining mechanical and chemical degradation factors. The impact of different operating circumstances on the formation of the SEI layer is simulated by the model. Further insights into health indicators and capacity thresholds for accurate RUL predictions were developed by Sun et al. [7], who used capacitance and resistance as primary health indicators and provided a third-order polynomial function to represent the degradation process.

Lui et al. [8] projected battery capacity deterioration by simulating the depletion of lithium inventory and active materials at both electrodes. The anticipated model incorporates the influences of temperature, state of charge, and current rates and offers a thorough understanding of battery aging.

Data-driven approaches, which use machine learning techniques that can handle big datasets and uncover hidden trends that are difficult for standard models to capture, forecast the battery SOH and RUL based on previous data and sophisticated algorithms.

In 2020, Gou et al. [9] presented a hybrid ensemble data-driven technique. To improve the prediction accuracy of SOH and RUL, the researchers combined nonlinear autoregressive models with random learning methods. In test datasets, their methodology performed better.

A time domain method was presented by Harris et al. [10] for monitoring SOH and RUL with the least amount of hardware. Their model uses a nonlinear least-squares method to estimate impedance characteristics by superimposing a short test signal on the battery load, whereas Reference [11] employed a support vector regression (SVR) model with a particle filter to manage measurement noise, yielding robust RUL predictions.

There are still a number of obstacles to overcome before precise and trustworthy SOH and RUL calculations can be obtained, even with the advances in model-based and data-driven approaches.

The complexity of battery aging processes poses a challenge for model-based approaches in identifying time-varying parameters and real-time applicability, as demonstrated by [12]. In their work, the authors [12] suggest a progressive LSTM technique to solve some of these issues with data quality and model fidelity.

Beganovic et al. [13] discussed the difficulties in developing accurate lifetime models that can adapt to varying operational conditions. They emphasize the need for models that can handle the stochastic nature of battery degradation. Additionally, Beganovic et al. [13] indicates that current methods are lacking the robustness required for real-world applications.

He et al. [14] pointed out the limitations of Gaussian process regression models in accurately predicting SOH and RUL without trend extraction. They proposed a multi-scale approach to improve prediction accuracy but noted that the complexity of battery degradation mechanisms still poses significant challenges.

Tang et al. [15] mentioned that data-driven methods can suffer from a lack of generalization and robustness due to the reliance on historical data. They propose an improved BiLSTM algorithm, yet acknowledge that the need for large, high-quality datasets remains a barrier. Gupta et al. [16] examined several machine learning methods for estimating SOH and RUL, stressing the benefits and drawbacks of each strategy. They came to the conclusion that although data-driven approaches have potential, combining them with physical models could improve their precision and dependability.

To increase prediction accuracy, Zhange et al. [17] suggested an ensemble approach that combines several data-driven models. They did point out that two important disadvantages are the requirement for a large amount of training data and the computational complexity.

There are distinct benefits to using both data-driven and model-based approaches for estimating SOH and RUL in battery systems. While data-driven methods use machine

learning algorithms and historical data to make precise forecasts, model-based methods offer insights into the physical and chemical processes of battery degradation [18,19].

In this work, a novel framework is introduced, the GRU-battery performance predictor (GRU-BPP), to overcome the drawbacks of both model-based and data-driven techniques. Granger causality and K-means clustering are used to comprehend inter-group linkages inside battery systems, while exploratory data analysis (EDA) and principal component analysis (PCA) analyze intra-group characteristics. The robust model captures complicated physical relationships and improves predicted accuracy by using gated recurrent unit (GRU) networks.

The structure of this paper is as follows: First, we give a summary of the dataset along with the experimental setup that was utilized to acquire the data in Section 2. We introduce our novel model GRU-battery performance predictor in Section 3. We explain the process of exploratory data analysis (EDA) to find significant trends and anomalies in the data in Section 3.1. The use of Granger causality to comprehend the temporal correlations between the battery parameters is covered next in Section 3.2. The principal component analysis (PCA) and clustering methods that are employed to classify the data and distinguish between different operational states are discussed in the next Section 3.3. Last, we present the complete flow chart of the GRU-battery performance predictor model (GRU-BPP) in Section 3.4 and assess its performance in comparison to benchmark techniques. We carry out a number of computational experiments in Section 4, such as Granger causality, principal component analysis (PCA), K-means clustering, and sensitivity analysis of the GRU-BPP hyperparameters. These analyses are performed on both the aging and reference performance testing (RPT) datasets. A review of the results is discussed in Section 6, and possible future research directions are included in the paper's conclusion in Section 7.

2. Dataset

This study utilizes a publicly accessible dataset compiled by [20]. The dataset includes aging data from three prismatic lithium-ion (Li-ion) battery cells tested across multiple aging rounds under a realistic forklift operation profile. Aging data from three prismatic lithium-ion battery cells comprise the dataset used in this investigation. During a two-week testing period, these cells underwent a realistic forklift operations profile that was distilled from a four-month stint of field operation. In order to expedite the aging process, experiments were carried out at 45 °C, 40 °C, and 35 °C for cells 1, 2, and 3, respectively. The forklift field operation's idling intervals were eliminated, and in order to comply with the battery test station's requirements, the charging and discharging current during the aging process was capped at 50 A. With the exception of the eliminated idling times, the state of charge (SOC) profile of the batteries throughout testing was identical to that of the field-operated forklift batteries. Every aging round consisted of two stages: a reference performance test (RPT) phase and an aging phase employing a realistic forklift load profile. For Cells 1 and 2 and for Cell 3, these phases were repeated 58 and 53 times, respectively. Throughout the aging and testing processes, precise data on current, voltage, energy, and temperature were captured on a second-by-second basis.

3. GRU-Battery Performance Predictor (GRU-BPP)

This paper introduces the GRU-battery performance predictor (GRU-BPP) as a novel data-driven approach specifically developed for this study to improve predictive accuracy and reliability in analyzing battery degradation. The new GRU-battery performance predictor (GRU-BPP) model combines physical and causal links to make predictions more accurate and reliable. It is used to study how batteries work and how they break down. The unique model makes use of sophisticated algorithms to comprehend the heterogeneity in battery performance under various operating situations. To find underlying trends, distributions, and anomalies in the dataset, exploratory data analysis, or EDA, is first carried out. In order to choose the most pertinent traits for further analysis, this stage is essential. The Granger causality test is then used to ascertain the temporal correlations

and predictive influences between the parameters. This test assesses the predictive power of previous values of one parameter over future values of another, hence shedding light on causal relationships within the data. The Granger causality test is based on a mathematical comparison of the variance of the residuals between the restricted model (which only includes lagged values of the predicted parameter) and the unconstrained model (which includes lagged values of both parameters). The F-statistic for Granger causality is calculated as

$$F = \frac{(RSS_r - RSS_u)/m}{RSS_u/(n - k - m)},$$

where the numbers m and n represent the number of lagged terms, k the number of parameters in the unrestricted model, and RSS_r the residual sum of squares for the limited and unrestricted models, respectively. Understanding the directional influence between factors and confirming that these associations hold true across various data subsets depend heavily on this approach. Next, principal component analysis (PCA) [21,22] is used to extract the most important features from the dataset while reducing its dimensionality. The data matrix X is broken down by the PCA into loadings and scores, resulting in $X = TP^T$, where the loadings are P and the scores are T . This method aids in pinpointing the main variables influencing battery degradation and performance. We may identify the variables that most significantly contribute to the observed variance by looking at the loadings of the principal components. This identifies important areas that require additional investigation. Our method is unusual in that it uses Granger causality and PCA together to validate internal links between the most crucial elements. By ensuring that the selected characteristics have both predicted causal linkages and a large contribution to the variance in the data, this dual synthesis improves the robustness of our model. By closely examining each feature's significance, the prediction model's accuracy and dependability are increased as it concentrates on the most important variables. The PCA-transformed characteristics are used to divide the data into discrete groups using K-means clustering. Minimizing the within-cluster sum of squares is the goal of K-means clustering:

$$J = \sum_{k=1}^K \sum_{i \in C_k} \|x_i - \mu_k\|^2,$$

where C_k is the set of points in cluster k , and μ_k is the centroid or the average position of points in cluster k . This clustering addresses both intra-group and inter-group heterogeneity, allowing us to uncover patterns and variations within and between clusters. The clusters reveal different degradation behaviors and performance characteristics, providing a deeper understanding of battery health under varying conditions. Following the clustering, the output clusters are used as input features for the GRU model, enhancing its predictive capability by incorporating the discovered patterns and relationships. The GRU model, designed to capture temporal dependencies and complex relationships within the data, is particularly suited for time-series predictions. The GRU is mathematically defined as follows:

$$\mathbf{h}_t = (1 - \mathbf{z}_t) \odot \mathbf{h}_{t-1} + \mathbf{z}_t \odot \tilde{\mathbf{h}}_t,$$

where \mathbf{z}_t is the update gate, and $\tilde{\mathbf{h}}_t$ is the candidate activation. The update gate \mathbf{z}_t and reset gate \mathbf{r}_t are computed as

$$\mathbf{z}_t = \sigma(\mathbf{W}_z \mathbf{x}_t + \mathbf{U}_z \mathbf{h}_{t-1}),$$

$$\mathbf{r}_t = \sigma(\mathbf{W}_r \mathbf{x}_t + \mathbf{U}_r \mathbf{h}_{t-1}),$$

$$\tilde{\mathbf{h}}_t = \tanh(\mathbf{W} \mathbf{x}_t + \mathbf{U} (\mathbf{r}_t \odot \mathbf{h}_{t-1})),$$

where σ is the sigmoid function. To assess the model's performance, 80% of the data are used for training, while the remaining 20% are used for testing. Mean squared error (MSE) was used as the loss function and the Adam optimizer with a learning rate of 0.001 was used to train the model. In order to avoid overfitting, training was carried out for 50 epochs with early termination. The model's performance was measured using RMSE on a different test

set that included 20% of the data. In order to comprehend intra- and inter-group differences and explain the variety in battery performance and degradation patterns, the relevance of the detected clusters was investigated. The present analysis offers a more profound understanding of the variables impacting battery health, guaranteeing that variation within and between groups is adequately addressed. The outcomes show how well the GRU-BPP model works at making accurate predictions, which improves knowledge and battery health management. The study's integration of sophisticated analytical approaches results in the identification of critical parameters that impact battery performance, as well as their utilization to construct a resilient prediction model. This all-encompassing strategy guarantees precise and trustworthy forecasts, significantly advancing the fields of degradation analysis and battery health monitoring. The higher performance of our unique methodology is demonstrated by comparing the GRU-BPP model with conventional methods like LME (statsmodels version: 0.14.0) and XGBoost. (xgboost version: 1.7.3).

3.1. Exploratory Data Analysis (EDA)

In this section, we go into the exploratory data analysis (EDA) of the dataset [20] to uncover initial patterns, trends, and insights. The following plots (Figures 1 and 2) illustrate various aspects of the data collected during the reference performance testing (RPT) and aging processes.

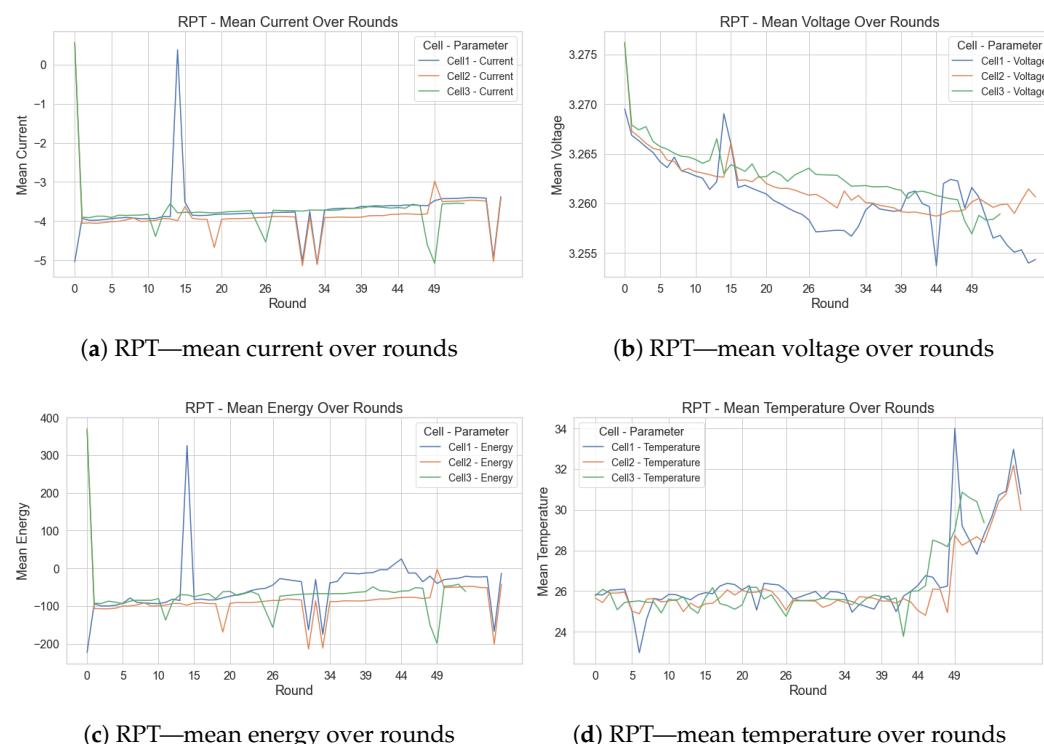


Figure 1. Reference performance testing (RPT) metrics over rounds for Cells 1, 2, and 3.

Figure 1a shows the mean current for Cells 1, 2, and 3 over multiple rounds of RPT. All cells initially exhibit a high mean current which stabilizes over time. Notably, Cell 1 shows significant fluctuations, indicating possible anomalies. Figure 1b presents the mean voltage trends, where all cells start with high initial voltages that decrease over time. Cell 1's voltage exhibits pronounced fluctuations, suggesting irregularities in its aging process. In Figure 1c, the mean energy data follow similar trends, with initial high values that decrease over time. Cell 1's energy data also show significant fluctuations, reinforcing the possibility of anomalous events. Figure 1d displays the mean temperature trends, which increase over time, particularly for Cell 1, indicating more significant degradation or potential testing issues.

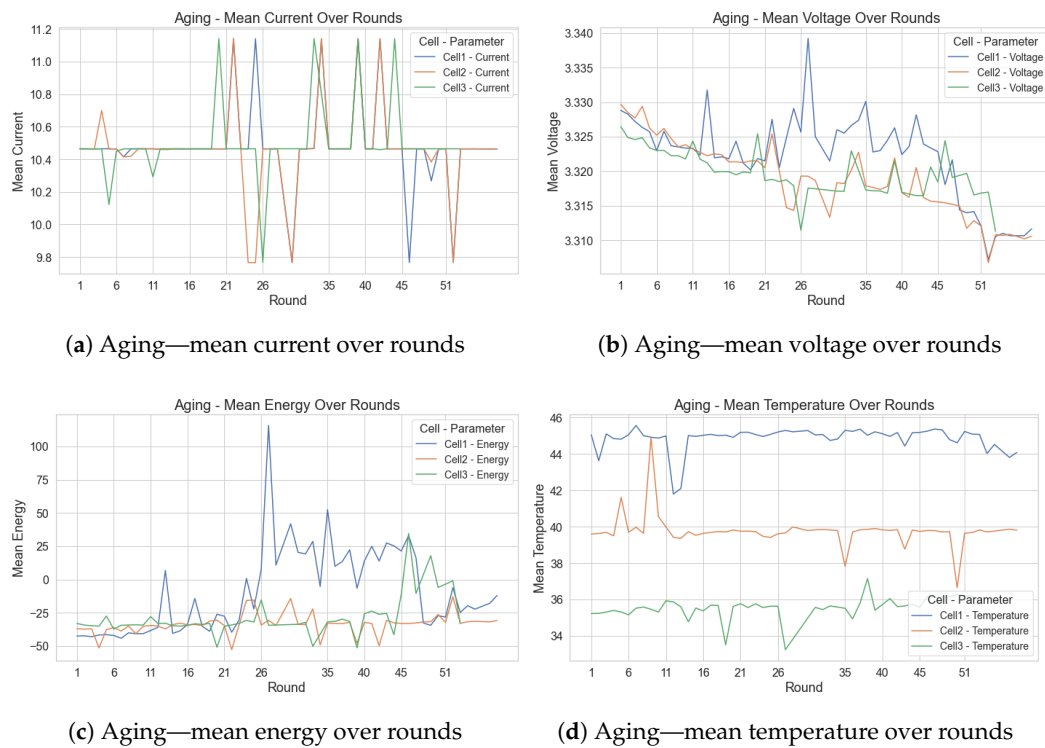


Figure 2. Aging metrics over rounds for Cells 1, 2, and 3.

During the aging process, as shown in Figure 2a–d, the mean current and voltage exhibit stable trends with minor fluctuations. Cell 1 shows more variability compared to Cells 2 and 3, indicating potential differences in response to aging. The energy and temperature trends during aging also reveal a declining pattern, with Cell 1 showing more significant fluctuations and higher temperatures, reflecting higher internal resistance and accelerated degradation.

Figure 3a–d show the distributions of current, voltage, energy, and temperature during RPT. The current distribution reveals peaks around specific values, indicating consistent loading during testing. Voltage readings fall within a narrow range, suggesting stable voltage levels. Energy values display a broad distribution, reflecting varying operational modes. Temperature readings cluster around 25 °C to 30 °C, with Cell 1 operating at slightly higher temperatures.

Figure 4a–d display the distributions of the same parameters during the aging process. Current and voltage distributions are similar to the RPT phase, indicating consistent loading and voltage ranges. Energy values show broader distributions, reflecting varying energy profiles during aging. Temperature distributions highlight distinct peaks, with Cell 1 experiencing higher and more variable temperatures, indicating greater degradation stress.

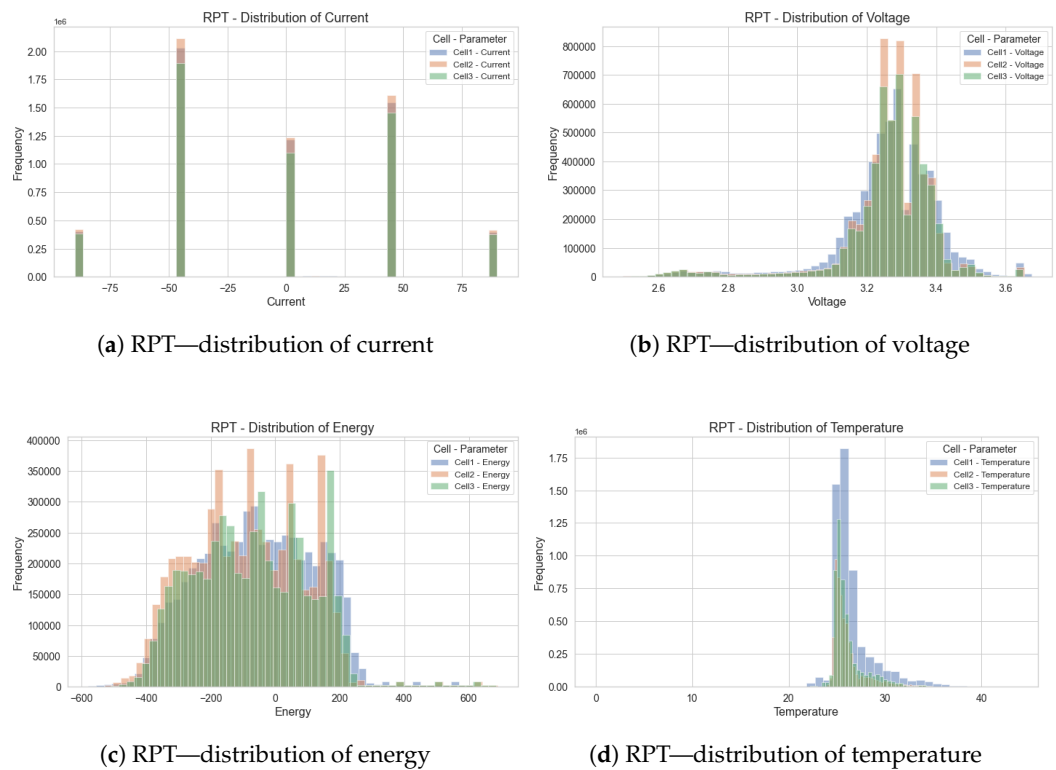


Figure 3. Distribution of current, voltage, energy, and temperature during reference performance testing (RPT) for Cells 1, 2, and 3.

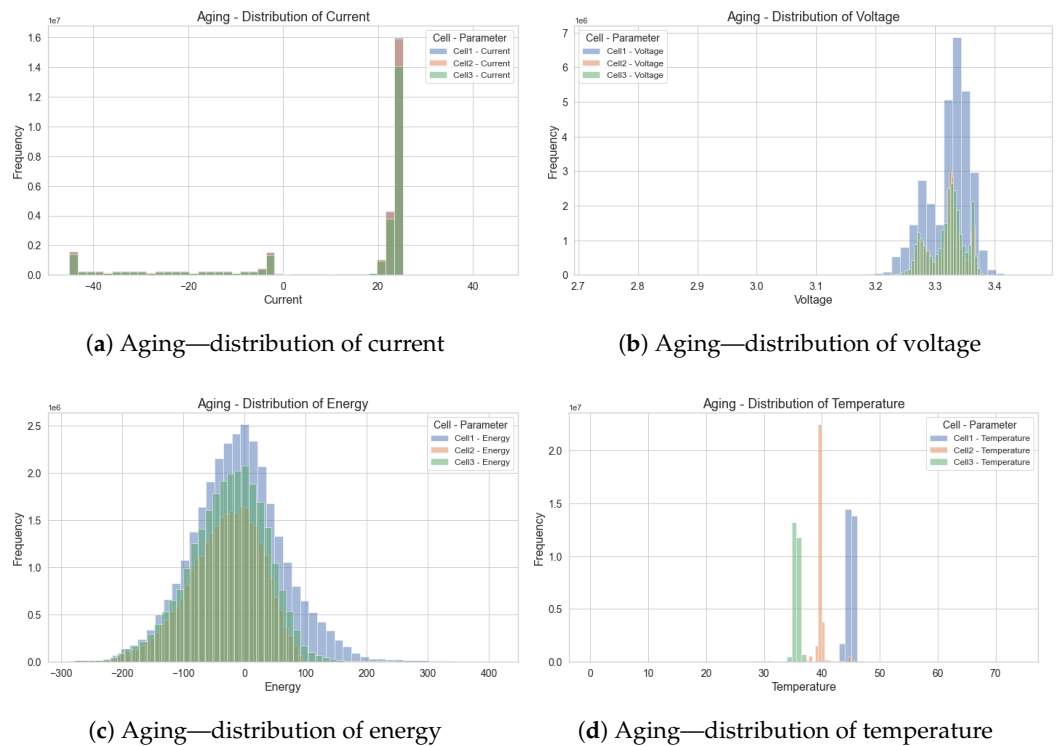


Figure 4. Distribution of current, voltage, energy, and temperature during aging for Cells 1, 2, and 3.

3.2. Granger Causality Analysis

The Granger causality test was applied to identify significant causal relationships between parameters by assessing the predictive capability of one parameter over another, using lags from 1 to 5. The analysis revealed significant relationships within both the RPT and aging data samples. In the RPT data, strong causal relationships were observed between current and voltage in Cell 2 and Cell 3 and between temperature and energy in Cell 2 (Table 1). For the aging data, notable relationships included those between temperature and energy in Cell 1 and between voltage and current in Cell 3 (Table 2). These interdependencies are crucial for subsequent PCA and clustering analyses, enhancing the predictive capabilities and reliability of battery health monitoring systems.

Table 1. Significant Granger causality relationships in RPT data samples.

Cell	Parameter_1	Parameter_2	Lag	p-Value
Cell2	Current	Voltage	3	0.047199
Cell2	Current	Voltage	4	0.024506
Cell2	Current	Voltage	5	0.043433
Cell3	Current	Voltage	3	0.017610
Cell3	Current	Voltage	4	0.039770
Cell2	Temperature	Energy	2	0.047331

Table 2. Significant Granger causality relationships in aging data samples.

Cell	Parameter_1	Parameter_2	Lag	p-Value
Cell2	Current	Temperature	1	0.042298
Cell3	Voltage	Current	5	0.015730
Cell2	Energy	Voltage	1	0.030174
Cell2	Temperature	Voltage	3	0.043914
Cell1	Temperature	Energy	1	0.012634
Cell1	Temperature	Energy	2	0.034834

3.3. PCA and Clustering Techniques

Principal component analysis (PCA) is employed here to capture the intra-group characteristics in order to examine complicated physical relationships. To further explore patterns within the dataset, clustering techniques were applied using K-means and Gaussian mixture models (GMM). The performance of both methods was evaluated using the Davies–Bouldin index, Calinski–Harabasz index, and silhouette score. Additionally, the plots of both methods are shown in Figures 5 and 6.

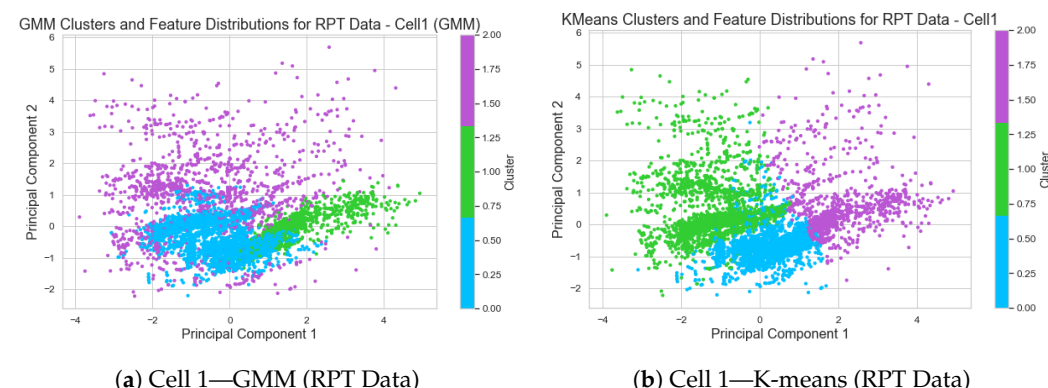


Figure 5. Cont.

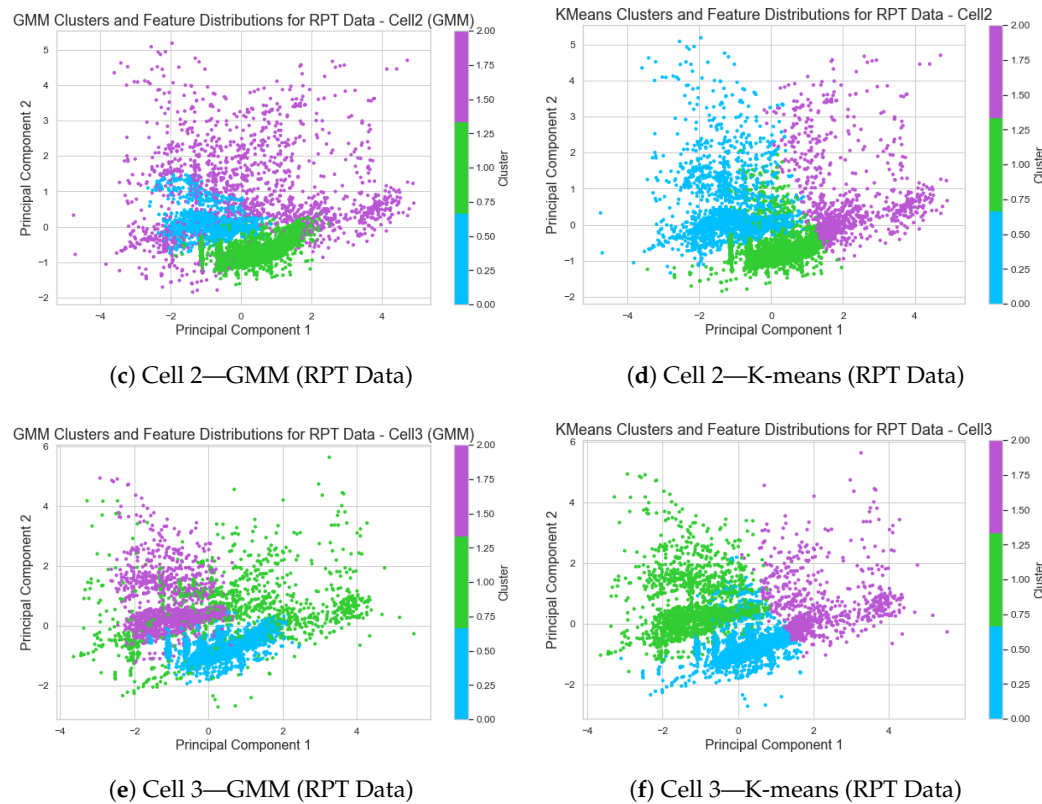


Figure 5. K-means and GMM clustering for RPT data across Cells 1, 2, and 3.

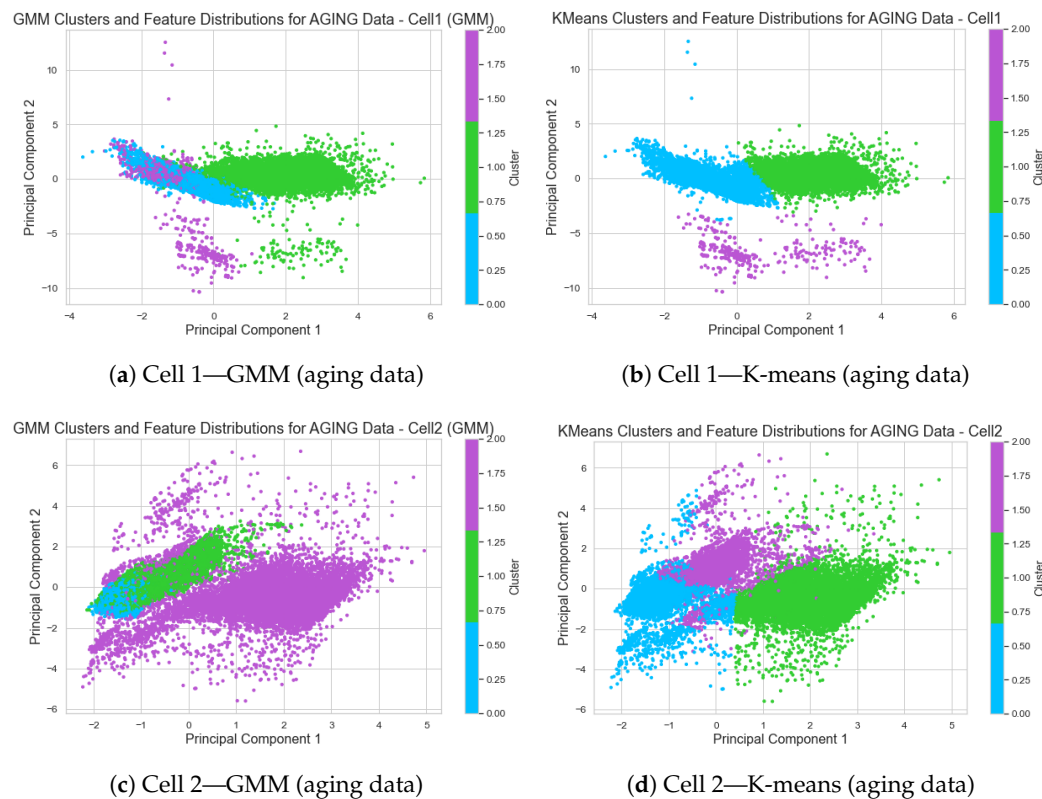


Figure 6. Cont.

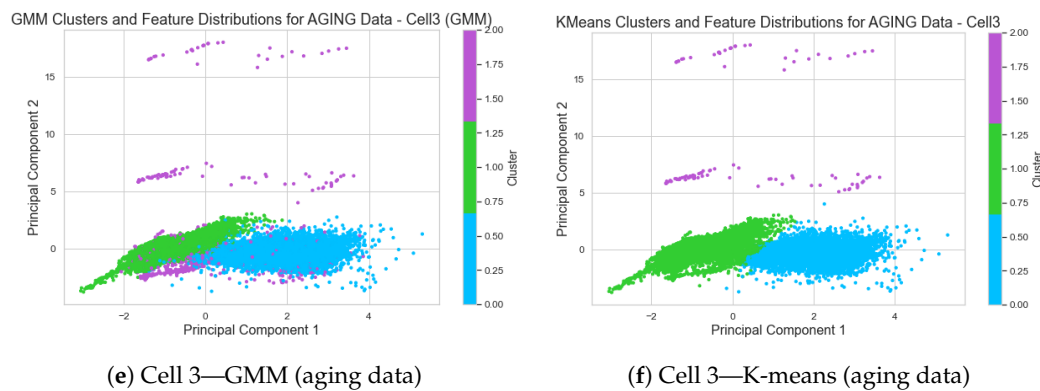


Figure 6. K-means and GMM clustering for aging data across Cells 1, 2, and 3.

K-means outperformed GMM, as indicated by lower Davies–Bouldin index and higher Calinski–Harabasz index and silhouette scores, suggesting more compact and well-separated clusters (Table 3). Consequently, K-means was selected for further analysis.

Table 3. Validation metrics for K-means and GMM clustering.

Method	Dataset	Davies–Bouldin Index	Calinski–Harabasz Index	Silhouette Score
K-means	RPT	1.2507	62,314.0320	0.65
	Aging	1.1136	475,508.1437	0.60
GMM	RPT	2.2019	25,275.9928	0.45
	Aging	1.1944	359,132.6545	0.55

3.4. Gated Recurrent Unit (GRU) Algorithm

A gated recurrent unit (GRU) is a type of recurrent neural network (RNN) designed to handle sequential data and capture temporal dependencies. GRUs address the vanishing gradient problem common in standard RNNs, with the reset gate and update gate determining the amount of past information retained and new information added. The GRU is defined mathematically as follows:

$$r_t = \sigma(W_r \cdot [h_{t-1}, x_t])$$

$$z_t = \sigma(W_z \cdot [h_{t-1}, x_t])$$

$$\tilde{h}_t = \tanh(W \cdot [r_t * h_{t-1}, x_t])$$

$$h_t = (1 - z_t) * h_{t-1} + z_t * \tilde{h}_t$$

where x_t is the input at time step t , h_{t-1} is the hidden state from the previous time step, σ is the sigmoid activation function, and W_r , W_z , and W are weight matrices. The GRU's ability to capture long-term dependencies makes it effective for time-series prediction tasks, such as forecasting the state of health (SOH) of lithium-ion batteries. The clustering outputs serve as additional input features for the GRU model, leveraging the identified patterns to enhance predictive accuracy. A flow chart explaining all the previous steps connecting the different phases of the novel approach is illustrated in the detailed flow chart in Figures 7 and 8.

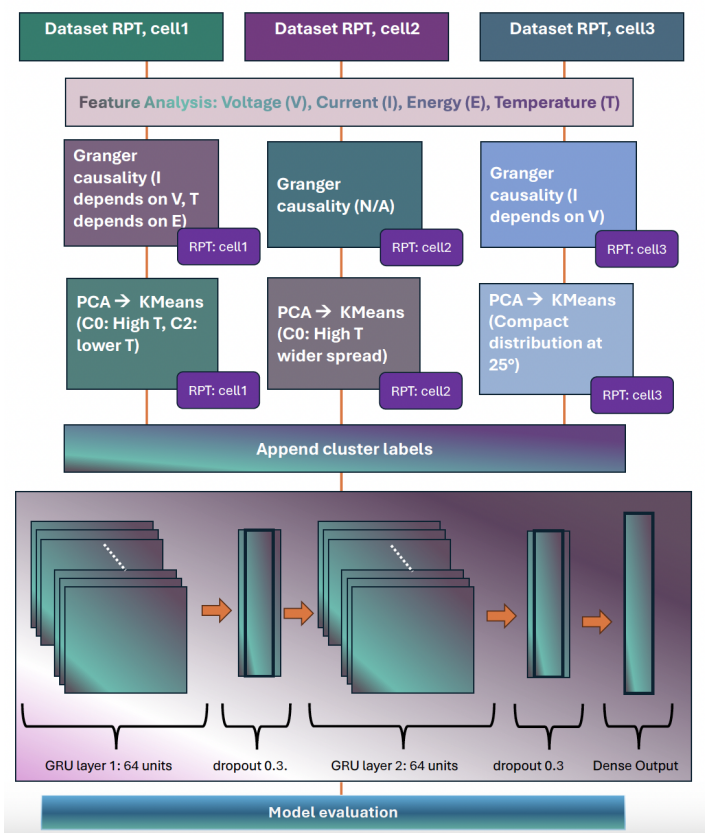


Figure 7. Flow Chart Details for RPT Dataset—Cell 1, 2, and 3.

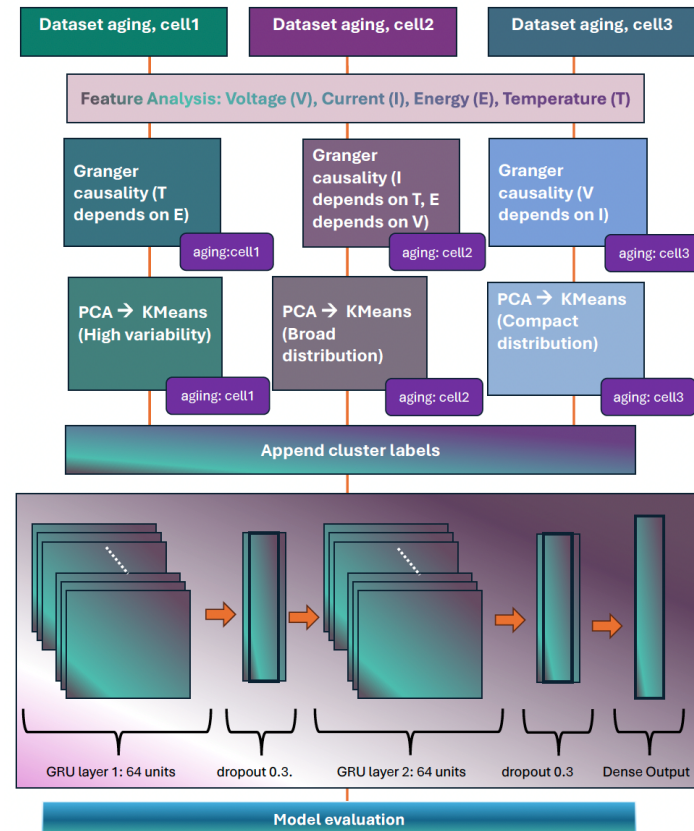


Figure 8. Flow chart details for aging dataset—Cell 1, 2, and 3.

4. Evaluation Results

In this section we evaluate our methods empirically as follows:

4.1. Principal Component Analysis

To further investigate the relationships and variance in the dataset, principal component analysis (PCA) was conducted on the standardized data. The PCA was applied separately to the RPT and aging datasets for each cell. The results are explained in Figures 9 and 10, respectively.

The data were first standardized to ensure that each feature contributed equally to the PCA. The top two principal components (PCs) were extracted and analyzed for each cell, providing insights into the key features driving the variance in the dataset. The contribution of each feature—current, voltage, energy, and temperature—to the principal components was visualized using bar plots.

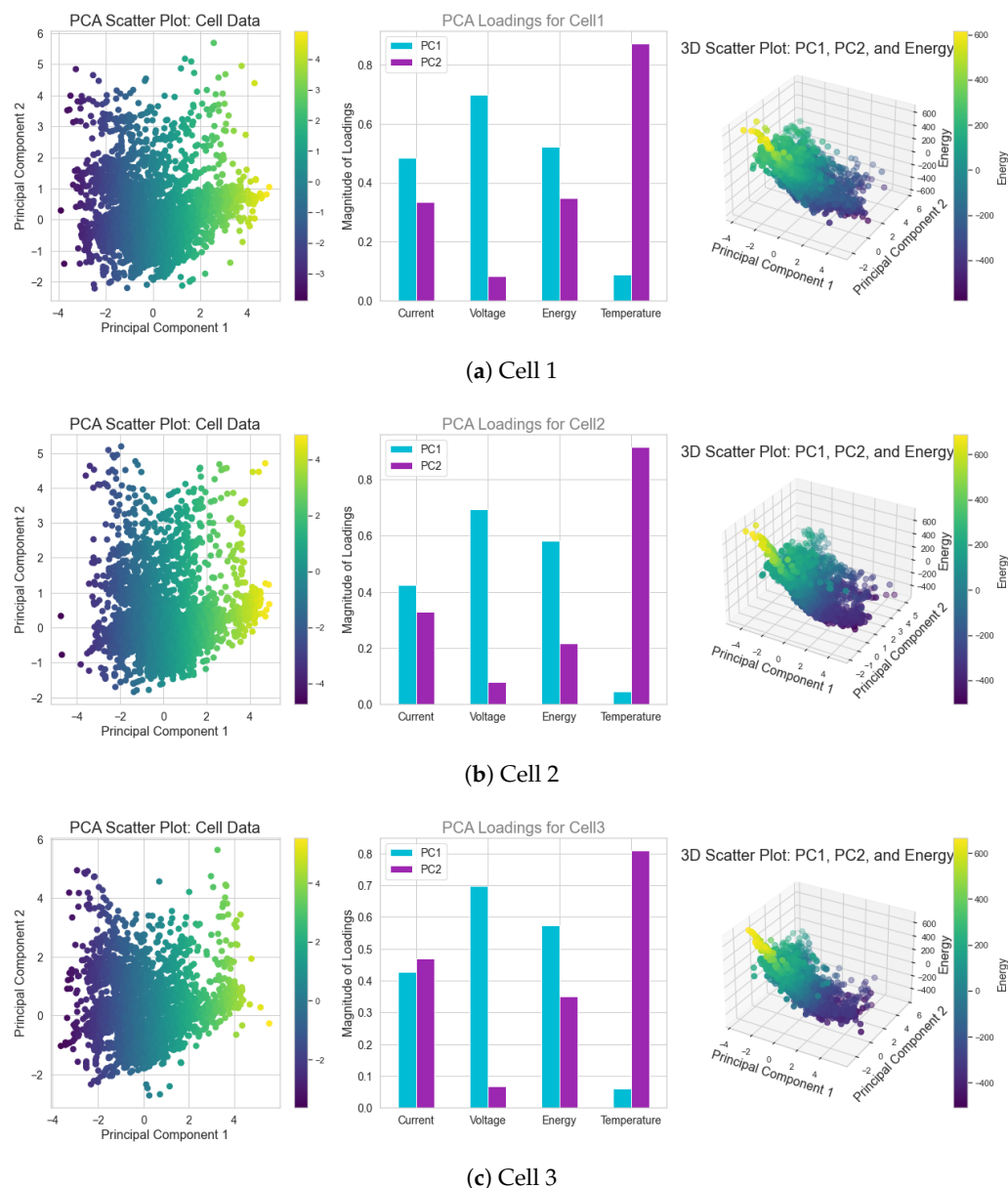


Figure 9. PCA, features, and energy contribution of RPT data for Cells 1, 2, and 3.

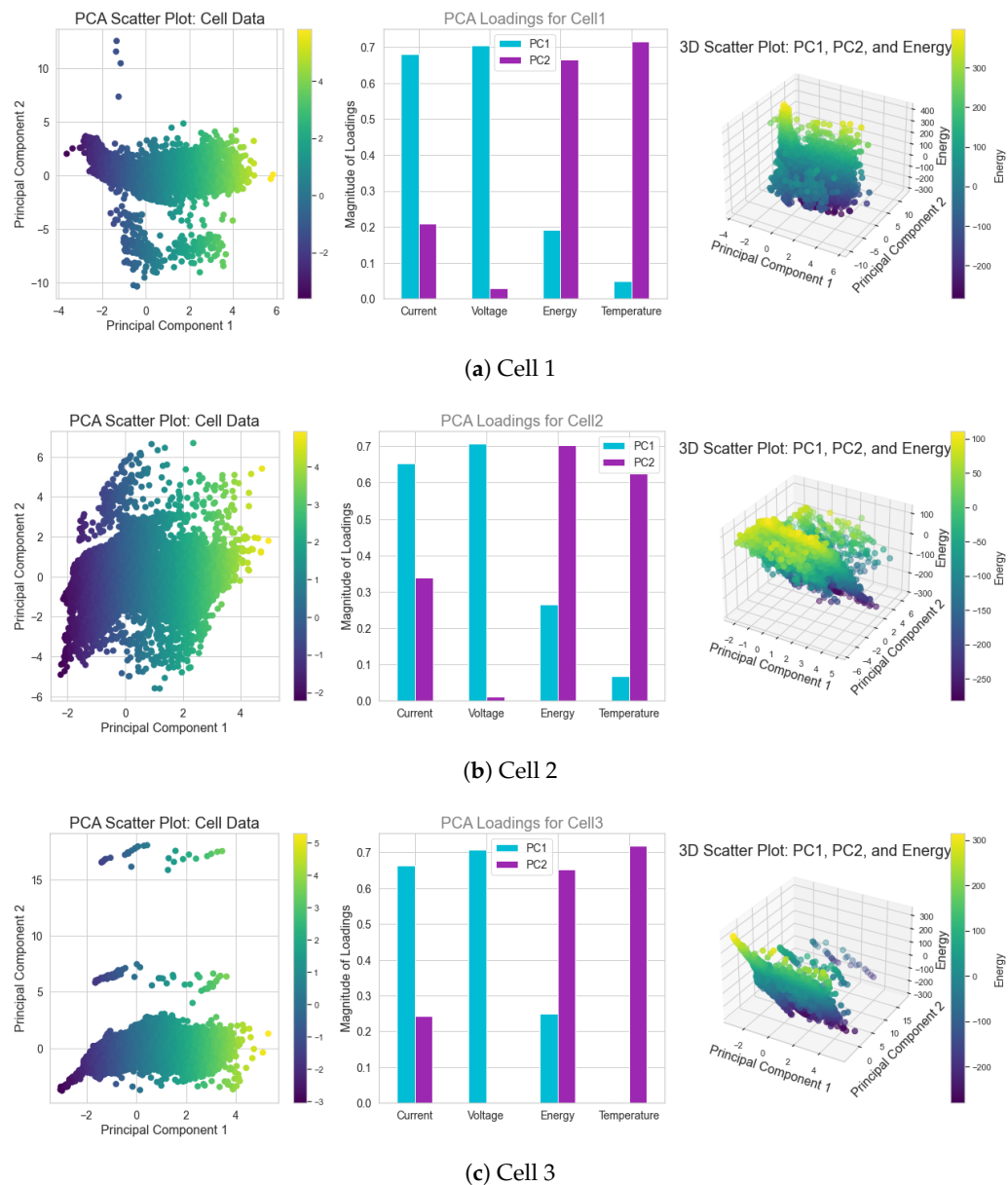


Figure 10. PCA, features, and energy contribution of aging data for Cells 1, 2, and 3.

The PCA plots' comparison analysis is displayed in Figure 9. PC1 has determined that the features of voltage and energy are the most prominent in Cells 1, 2, and 3, while PC2 has demonstrated that temperature is the most important feature. Cell 1, which was tested at 45 °C, displays a distribution of data points along both principal components in the PCA scatter plot. This suggests that there is a significant amount of variability in the dataset and that higher temperatures may be causing more pronounced degradation effects, which in turn may lead to greater variability in the battery's performance during the RPT process. In contrast to Cell 3, the PCA scatter plot for Cell 2, which is aged at a moderate temperature of 35 °C, shows a more scattered distribution of data points. This points at increased unpredictability as well as possible deterioration in the battery's functionality under these particular circumstances. In its PCA scatter plot, Cell 3, which was aged at a lower temperature of 25 °C, displays a more compact distribution of data points, indicating steady and reliable performance. A strong response to the aging conditions and little variability are suggested by the clustering around the principal components. Lower temperatures seem to lessen the impacts of degradation, resulting in more dependable performance throughout the RPT procedure. Comparative examination of the PCA plots

for Cells 1, 2, and 3 in Figure 10 also showed different patterns. The PCA scatter plot for Cell 1 shows a distribution with compact variance along both major components, indicating a high degree of response variability from the battery. The bar plot shows that for PC2, temperature and energy are dominant features, while for PC1, voltage and current remain significant. Referencing Table 2, the significant Granger causality relationships in Cell 1 between temperature and energy align with the PCA results, reinforcing the importance of these parameters.

For Cell 2 in Figure 10b, the PCA scatter plot displays a very broad distribution, indicating substantial variability. This suggests higher variability and potential stress or degradation in the battery's performance under its specific conditions. The bar plot shows that for PC1, current and voltage are dominant features, while for PC2, energy and temperature are significant. Referencing Table 2, the significant Granger causality relationships in Cell 2 between current and temperature, energy and voltage, and temperature and voltage align with the PCA results, highlighting the critical role of these parameters.

For Cell 3 in Figure 10c, the PCA scatter plot shows a compacted distribution compared to Cell 2, indicating relatively stable performance. The clustering around the principal components suggests minimal variability. The bar plot shows that for PC1, current and voltage are dominant features, while for PC2, temperature and energy are significant. Referencing Table 2, the significant Granger causality relationships in Cell 3 between voltage and current align with the PCA results, confirming the importance of these parameters.

Additionally, the Figures 9 and 10 visualize the interaction between the principal components (PC1, PC2) and the energy feature. By including energy on the z-axis, the 3D plots provide a clearer understanding of how energy levels distribute across different regions of the PCA space. For instance, in the 3D scatter plot of RPT data for all cells, the energy values show a distinct gradient, with higher energy clustering in the lower ranges of PC1 and PC2, as shown in Figure 9, suggesting a concentration of higher energy data points under these component conditions. In contrast, Cells 1 and 2 in the Figure 10 plots reveal more evenly distributed energy levels across the PCA components, further highlighting its stability and consistent performance.

4.2. Feature Distribution in K-Means Clustering

In this computational experiment, we discuss the features distribution in each cluster for the RPT and aging datasets in Cells 1, 2, and 3. The distinct clusters are visualized in the right plots (b, d, and f) of Figures 5 and 6.

The clusters are well separated in the principal component space, indicating clear patterns in the battery's operational data. Further analysis of the feature distributions within each cluster (Figure 11) shows significant differences in current, voltage, energy, and temperature.

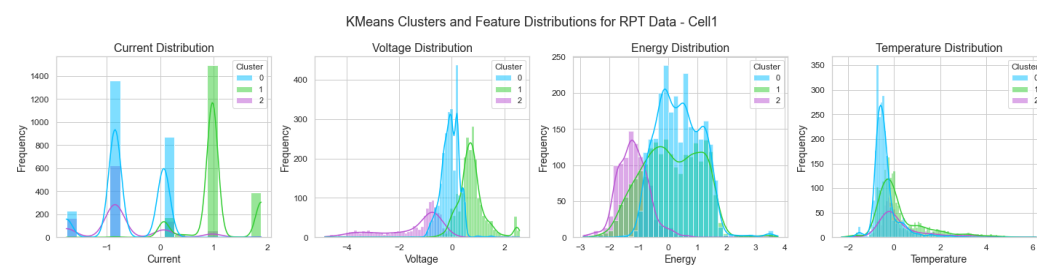


Figure 11. Feature distributions for RPT data clusters—Cell 1.

In Cell 1, the current distribution in Figure 11 highlights that Cluster 0 (blue) has prominent current peaks, suggesting periods of inactivity or low current flow. In contrast, Clusters 1 (green) and 2 (purple) display more varied distributions, indicating different current levels during operation. The voltage distribution is tightly clustered around central values, with Cluster 1 (green) showing a slightly wider spread, suggesting more variability in voltage levels. The energy distribution reveals that Cluster 0 (blue) and Cluster 1 (green)

have a more spread-out distribution, while Cluster 2 (purple) shows a distinct peak, representing energy storage. Temperature distributions indicate that Cluster 0 (purple) operates at higher temperature ranges compared to the other clusters. This could be due to different thermal conditions or varying states of health, impacting the battery's performance.

For Cell 2, the K-means clustering is shown in Figure 5d; the corresponding feature distributions in Figure 12 again demonstrate distinct characteristics in current, voltage, energy, and temperature for each cluster. Clear prominent peaks are shown in Cluster 1 for current, voltage, energy, and temperature.

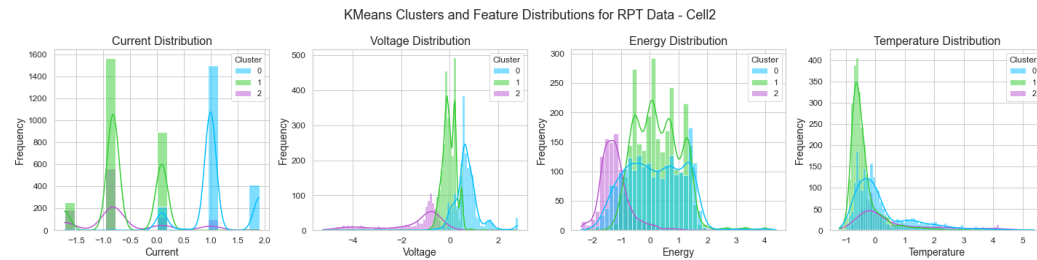


Figure 12. Feature distributions for RPT data clusters—Cell 2.

Similarly, for Cell 3, Figure 5f shows the clusters in the PCA space, while Figure 13 illustrates the feature distributions. The patterns in Cluster 0 observed here are similar to the ones in Cluster 1 in Cell 2.

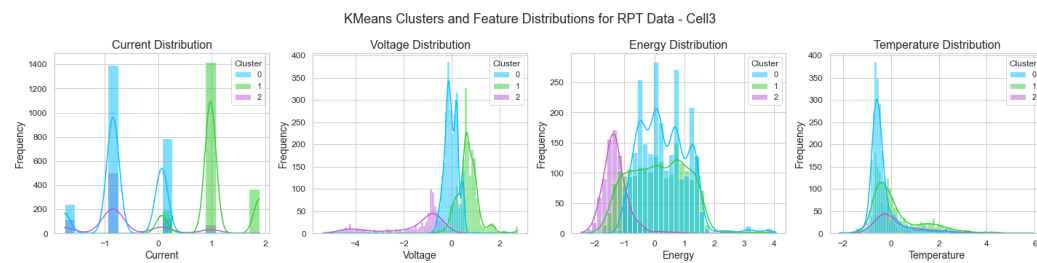


Figure 13. Feature distributions for RPT data clusters—Cell 3.

The K-means clustering for the aging data of Cell 1, as shown in Figure 6b, reveals three distinct clusters. Cluster 0 (blue), Cluster 1 (green), and Cluster 2 (purple).

The feature distributions in Figure 14 further show these clusters. Cluster 0 predominantly exhibits higher values in voltage and energy in Cell 1, mostly aligning with its distribution in the PCA plot. In Figure 15 Cluster 1 shows a broader distribution across voltage and energy in Cell 2. Cell 3 in Figure 16 has similar distribution across voltage and energy in Cluster 1, highlighting its diverse characteristics.

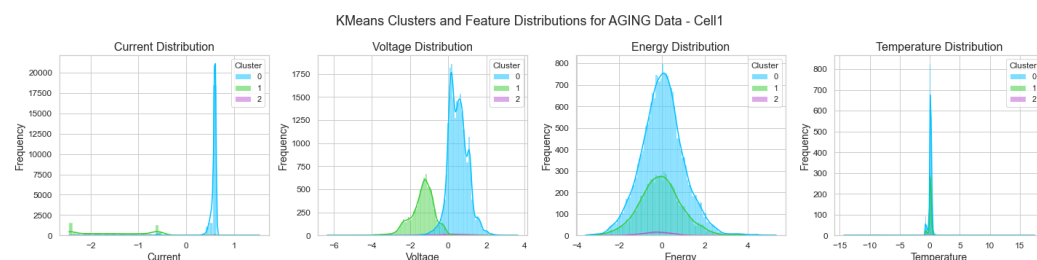


Figure 14. Feature distributions for aging data clusters—Cell 1.

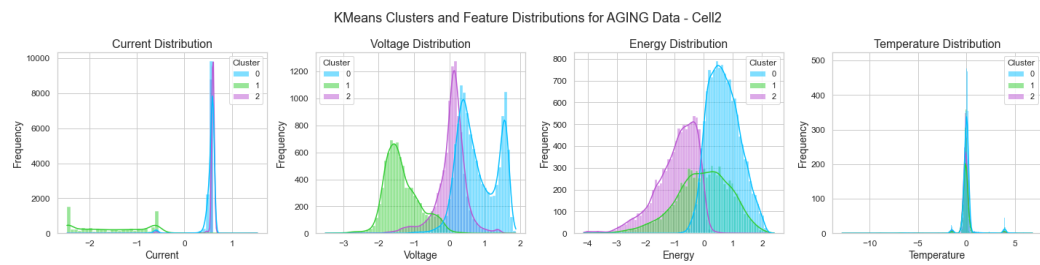


Figure 15. Feature distributions for aging data clusters—Cell 2.

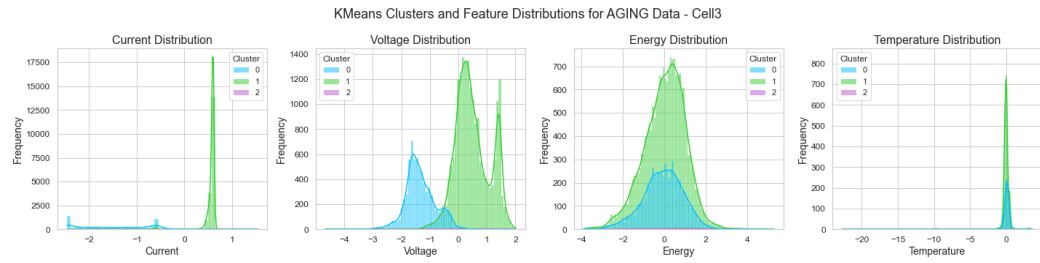


Figure 16. Feature distributions for aging data clusters—Cell 3.

5. Sensitivity Analysis for the RPT and Aging Dataset Using the GRU-BPP Archticture

5.1. Sensitivity Analysis for RPT Data

According to Table 4, it is possible to have over-regularization and suboptimal generalization when the batch size or dropout rate is increased. For example, when the batch size is 64 and the dropout rate is 0.5, the RMSE value is 0.1835 with R^2 equal to 0.9160. On the other hand, a lower batch size of 32 and a 0.3 dropout rate result in a higher R^2 of 0.963 and an improved RMSE of 0.1561, indicating better performance.

To this end, 64 hidden units, a learning rate of 1, a batch size of 32, and a dropout rate of 0.3 are the ideal settings for the RPT dataset. This configuration results in the greatest R^2 value (0.963) and one of the lowest RMSE at (0.1561). In order to improve the accuracy and generalizability of the RPT predictions, a smaller batch size and a modest dropout rate are advised.

Table 4. RPT sensitivity analysis results.

Hidden Units	Learning Rate	Batch Size	Dropout Rate	RMSE	MAE	R^2
64	1	32	0.3	0.1561	0.1115	0.963
64	1	32	0.5	0.1610	0.1208	0.9673
64	1	64	0.3	0.1504	0.0986	0.9141
64	1	64	0.5	0.1835	0.1519	0.9160
64	0.01	32	0.3	0.1559	0.1117	0.9361
64	0.01	32	0.5	0.1596	0.1182	0.9468
64	0.01	64	0.3	0.1603	0.1168	0.9570
64	0.01	64	0.5	0.1694	0.1334	0.9922
128	1	32	0.3	0.1502	0.0967	0.9147
128	1	32	0.5	0.1509	0.0936	0.9254
128	1	64	0.3	0.1562	0.1115	0.9985
128	1	64	0.5	0.1651	0.1262	0.9265
128	0.01	32	0.3	0.1514	0.1022	0.9314
128	0.01	32	0.5	0.1504	0.0988	0.9177
128	0.01	64	0.3	0.1553	0.0992	0.9854
128	0.01	64	0.5	0.1509	0.1001	0.9250

5.2. Sensitivity Analysis for Aging Data

The aging sensitivity analysis in Table 5 shows that a smaller batch size combined with a dropout rate of 0.3 provides better performance, with lower RMSE and higher R^2 values.

The optimal configuration appears to be 64 hidden units, a learning rate of 1, a batch size of 32, and a dropout rate of 0.3, yielding an RMSE of 0.0321 and an R^2 of 0.944.

In contrast, increasing the dropout rate to 0.5 or using larger batch sizes typically results in a slight reduction in performance. The configuration of 128 hidden units, a learning rate of 1, and a batch size of 64, for example, resulted in a higher RMSE of 0.0398 and a lower R^2 of 0.944, confirming that smaller batch sizes and moderate dropout rates are more effective for aging data.

In both the RPT and aging datasets, smaller batch sizes and moderate dropout rates consistently lead to better model performance. However, the aging dataset exhibits more stable and lower RMSE values overall compared to the RPT dataset, suggesting that it is less sensitive to variations in hyperparameters. The trends in how dropout rates and batch sizes affect accuracy remain similar in both datasets, though the aging data show less variability in performance.

Table 5. Aging sensitivity analysis results.

Hidden Units	Learning Rate	Batch Size	Dropout Rate	RMSE	MAE	R^2
64	1	32	0.3	0.0321	0.0253	0.944
64	1	32	0.5	0.0321	0.0257	0.919
64	1	64	0.3	0.0334	0.0285	0.964
64	1	64	0.5	0.0321	0.0259	0.934
64	0.01	32	0.3	0.0327	0.0247	0.942
64	0.01	32	0.5	0.0321	0.0250	0.905
64	0.01	64	0.3	0.0351	0.0305	0.985
64	0.01	64	0.5	0.0332	0.0249	0.975
128	1	32	0.3	0.0322	0.0249	0.971
128	1	32	0.5	0.0321	0.0257	0.915
128	1	64	0.3	0.0398	0.0350	0.944
128	1	64	0.5	0.0338	0.0252	0.994
128	0.01	32	0.3	0.0323	0.0247	0.981
128	0.01	32	0.5	0.0321	0.0256	0.949
128	0.01	64	0.3	0.0386	0.0339	0.947
128	0.01	64	0.5	0.0321	0.0254	0.910

For both the RPT and aging datasets, the sensitivity analysis indicates that a smaller learning rate (0.01) and a moderate dropout rate (0.3) are more effective in maintaining model accuracy. Additionally, simpler models with 64 hidden units tend to perform better, achieving lower RMSE and higher R^2 values. Increasing the model complexity or regularization (i.e., higher dropout rates) generally leads to diminishing returns, as seen in the increased test losses and lower R^2 values. Based on these results, a smaller, simpler GRU architecture with moderate regularization and a learning rate of 0.01 is recommended for both datasets.

5.3. Comparative Evaluation of Test Losses and Validation for RPT and Aging Datasets

The graphs in Figure 17 show the test and validation losses for the RPT and aging datasets over 50 epochs. A steadily reduction over 20 epochs can be noticed in the validation loss of the RPT dataset. On the other side, the aging dataset has a significant reduction in the validation loss during the first 5 epochs; the curve stabilizes after that. Through the same comparison, we can see that similar behavior is shown for the testing loss in the aging and RPT datasets, the test losses for both datasets show similar patterns during validation.

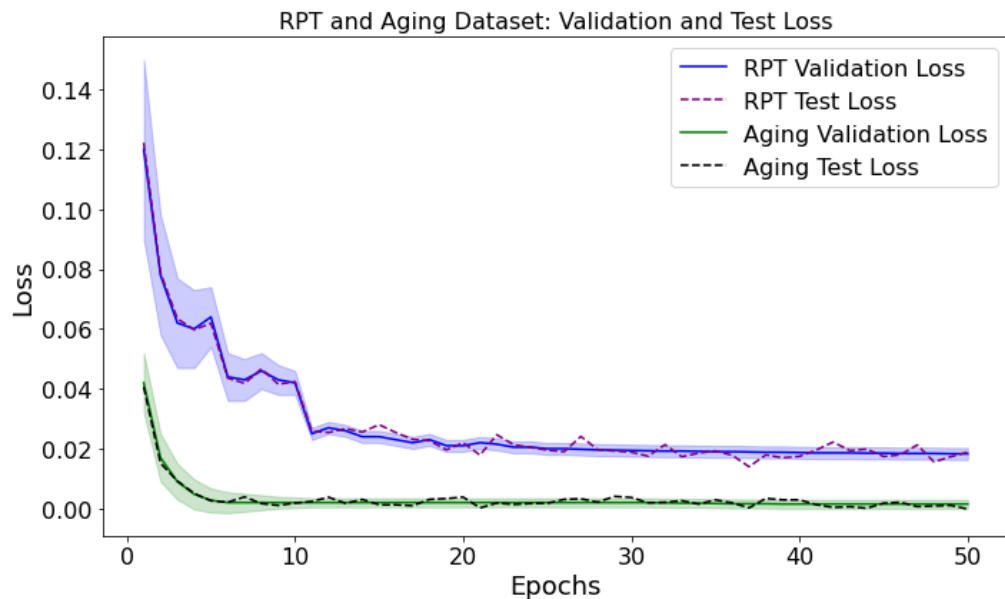


Figure 17. Validation loss and testing loss results for the GRU-BPP model on the RPT and aging datasets.

5.4. Performance Comparison of Different Models

Table 6 shows the RMSE, MAE, and R^2 values for the reference performance testing (RPT) and aging datasets. The hyperparameters selection for each model are shown in Table 7.

Table 6. Comparison of Performance Metrics for Different Models.

Model	Dataset	RMSE	MAE	R^2
LME	RPT	0.7998 ± 0.0100	0.5500 ± 0.0120	0.8999
	Aging	0.5047 ± 0.0150	0.3700 ± 0.0160	0.9213
GRU	RPT	0.9206 ± 0.0250	0.4760 ± 0.0510	0.8406
	Aging	0.1114 ± 0.0543	0.1030 ± 0.0310	0.8801
Bi-LSTM	RPT	0.9289 ± 0.0260	0.4810 ± 0.0520	0.8355
	Aging	0.1462 ± 0.0011	0.0949 ± 0.0013	0.8244
Attention-LSTM	RPT	0.9163 ± 0.0240	0.4675 ± 0.0490	0.8429
	Aging	0.1478 ± 0.0013	0.0992 ± 0.0014	0.8276
LSTM	RPT	0.9423 ± 0.0500	0.5000 ± 0.0500	0.8333
	Aging	0.6375 ± 0.0800	0.4560 ± 0.0810	0.7771
XGBoost	RPT	0.2492 ± 0.0050	0.1900 ± 0.0051	0.9651
	Aging	0.1101 ± 0.0030	0.0900 ± 0.0030	0.9884
GRU-BPP	RPT	0.1667 ± 0.0020	0.1286 ± 0.0170	0.9888
	Aging	0.0321 ± 0.0035	0.0253 ± 0.0040	0.9901
ANN	RPT	1.0800 ± 0.1000	0.9000 ± 0.1000	0.7501
	Aging	0.5000 ± 0.1200	0.4805 ± 0.2100	0.3237

The results of the GRU-BPP model outperforms all other models including Bi-LSTM and Attention-LSTM, achieving the lowest RMSE of 0.166694 for the RPT dataset and 0.032066 for the aging dataset. This captures the GRU-BPP's superiority in modeling the temporal dependencies in battery degradation data, making it a highly effective tool for SOH prediction in lithium-ion batteries.

Table 7. Hyperparameters for different models.

Model	Hyperparameters
LME	Fixed Effects: Current, Voltage, Temperature Random Effect: Cluster
Bi-LSTM	Units: 64 (bidirectional), Activation: ReLU Optimizer: Adam, Epochs: 50
Attention-LSTM	Units: 64, Activation: ReLU Attention Mechanism: Scaled Dot-Product Optimizer: Adam, Epochs: 50
LSTM	Units: 64, Activation: ReLU Optimizer: Adam, Epochs: 50
XGBoost	n_estimators: 100, learning_rate: 0.1 Objective: regression
GRU	Units: 64, Activation: ReLU Optimizer: Adam, Epochs: 50
Random Forest	n_estimators: 100, Criterion: MSE
K-means	n_clusters: 3, Random State: 42
GMM	n_components: 3, Covariance Type: Full Random State: 42
ANN	Layers: 3 Hidden Layers Units: 64 (Each Layer), Activation: ReLU Optimizer: Adam, Epochs: 50

6. Discussion

In this paper, important insights into the performance and degradation patterns of lithium-ion battery cells were obtained using the principal component analysis (PCA), Granger causality, and K-means clustering techniques on the reference performance testing (RPT) and aging datasets.

The Granger causality study improved our understanding of the temporal dynamics of battery degradation by revealing important causal links between important parameters like current, voltage, temperature, and energy. Strong causal relationships between current and voltage were found for the RPT dataset across a variety of lags, especially in Cells 2 and 3. This result is consistent with the physical characteristics of lithium-ion batteries, whose internal resistance causes current fluctuations to frequently occur before voltage changes. Furthermore, during short-term testing, substantial Granger causality correlations between temperature and energy were discovered in Cell 2, emphasizing the influence of thermal circumstances on energy dissipation. On the other hand, the aging dataset showed stronger correlations between energy and temperature as well as between voltage and current, especially in Cells 1 and 3. These results highlight the long-term implications of temperature on battery health, especially when considering the deterioration of cells over time.

The main characteristics causing variance in the dataset were successfully determined using the PCA analysis. Voltage and energy were found to be the most important features for PC1 in the RPT dataset, but temperature was more noticeable for PC2. According to these results, temperature has a minor but significant impact on short-term battery performance, but voltage and energy are the main predicting components in the process. The aging dataset shows a stronger temperature contribution to variance, particularly in PC2, which is indicative of the growing effect of heat on battery deterioration over time. This is especially clear in Cell 1, where the PCA scatter plots indicate that increased operating temperatures are linked to greater battery performance variability. The usefulness of PCA in feature selection and dimensionality reduction is demonstrated by its capacity to disclose these unique patterns under a variety of operating situations.

These conclusions were further supported by K-means clustering, which divided the data into discrete groups according to the PCA-transformed features. Differential distributions of current, voltage, energy, and temperature were used to generate unique clusters in the RPT dataset. Cell 1's Cluster 0 operated at higher temperatures, whereas Cells 2 and 3's Cluster 1 demonstrated more consistent performance. The distinct degradation behaviors under varied test settings are reflected in the clustering patterns. Comparably, in the aging dataset, the clusters showed different operating modes, and the clusters were mostly defined by voltage and energy. The temperature distributions in Cell 1 support the notion that heat is a primary cause of long-term damage by indicating that thermal management becomes more crucial as the battery matures.

The state of health (SOH) of lithium-ion batteries may now be predicted with a comprehensive framework of three techniques—Granger causality, PCA, and clustering—incorporated into the GRU-BPP model. In comparison with other machine learning models (such as GRU, LME, LSTM, and XGBoost), the GRU-BPP model performed better and obtained the lowest RMSE values for the RPT and aging datasets. This is explained by the model's suitability for time-series prediction tasks due to its capacity to capture both feature interactions and temporal dependencies. The model's capacity to learn from the found patterns was improved by using the clustering results as input features, which produced predictions that were more accurate.

A lower batch size and a moderate dropout rate (0.3) were found to be ideal for both datasets by the sensitivity analysis. Specifically, it was discovered that the optimal hyperparameters for the GRU-BPP model were 64 hidden units, a learning rate of 0.01, and a batch size of 32. Using 128 hidden units or a greater learning rate, for example, increased the model's complexity and caused overfitting, as shown by higher RMSE values. These results imply that for SOH prediction, a more straightforward model with moderate regularization works better.

To further illustrate the advantages and limitations of the GRU-BPP model compared to advanced deep learning techniques, we make the following key points as given in Table 8:

Table 8. Comparison of GRU-BPP with advanced deep learning models for battery life prediction based on general recent studies in different applications [23–26].

Model	Key Components	Advantages	Disadvantages
GRU-BPP	GRU + PCA, K-means, Granger Causality	Interpretability, captures intra- and inter-group dependencies, high accuracy	Limited in handling complex non-linearities
Attention-LSTM	LSTM with Attention mechanism	Captures long-range dependencies, high accuracy	Computationally intensive
Transformer	Self-attention, Multi-head Attention	Excellent for high-dimensional data, captures complex dependencies	High memory and computational demand
BiLSTM	Bidirectional LSTM layers	Effective in capturing context from both directions	Slower training, high parameter count

The GRU-BPP model offers important advantages in predicting SOH batteries, and it is important to recognize its strengths and limitations. One of the main advantages of the GRU-BPP model is its interpretability, as it incorporates Granger causality between key parameters (e.g., temperature and voltage) to provide insight into the causal relationships and thus improve the understanding of battery degradation mechanisms. In addition, PCA and clustering techniques allow GRU-BPP to capture the variability intra- and inter-groups, providing a structured approach to feature selection and improving the robustness of the model. This structured analysis allows the model to more effectively identify critical operating conditions and underlying degradation behavior, resulting in higher accuracy.

compared to some complex deep learning models. However, due to its simple structure, the GRU-BPP model may not be flexible enough to capture highly nonlinear dependencies and complex temporal patterns as other advanced deep learning models; however, for our study, GRU-BPP was an excellent choice for battery SOH prediction with causal insights. The table below summarizes the comparison between GRU-BPP and alternative deep learning models.

7. Conclusions

In this paper, we developed a novel GRU-battery performance predictor (GRU-BPP) model to forecast lithium-ion batteries' state of health (SOH). In order to pinpoint the critical elements affecting battery performance and deterioration, the model combines several intricate analytical techniques, including Granger causality, principal component analysis (PCA), and K-means clustering.

Significant causal correlations between current, voltage, temperature, and energy were found using the Granger causality analysis, which describes the temporal dynamics of battery degradation. Temperature was more important in the aging dataset, especially in the later phases of degradation, yet voltage and energy were found to be the primary drivers of variance in the dataset, as indicated by the PCA analysis.

Different degradation patterns were shown by the K-means clustering, with voltage and energy standing out as crucial characteristics in identifying the clusters. The GRU-BPP model was then able to better capture intra-group and inter-group patterns by using these clusters as input characteristics.

With the lowest RMSE values for the RPT and aging datasets, the GRU-BPP model outperforms conventional machine learning methods. The model was quite successful at predicting SOH because it could capture temporal dependencies and take advantage of clustered patterns. A more straightforward model with 64 hidden units, a learning rate of 0.01, and a dropout rate of 0.3 performed best, avoiding overfitting and retaining good accuracy, according to the sensitivity analysis.

Finally, the GRU-BPP model could provide a reliable and understandable way to forecast the health of lithium-ion batteries, by enhancing battery health monitoring, promoting energy efficiency, and sustainability, which has important ramifications for degradation analysis and battery health monitoring. This model is a useful resource for battery management systems and upcoming studies in this area since it not only increases prediction accuracy but also offers a deeper knowledge of the causes behind battery degradation. Further studies on additional datasets will be conducted to generalize the results on even wider temperature ranges, particularly lower operating temperatures.

8. Declaration of Generative AI and AI-Assisted Technologies

The authors acknowledge the use of Quillbot, an AI-assisted tool, during the preparation of this work, specifically to enhance the readability and language quality of the manuscript. The tool was employed to refine the clarity and coherence of the writing, ensuring that the manuscript effectively communicates the research findings. After utilizing this service, the authors thoroughly reviewed and edited the content to maintain the scientific integrity and accuracy of the work. They take full responsibility for the final content and conclusions presented in the article.

Author Contributions: Conceptualization, S.Q. and A.P.; Methodology, S.Q.; Software, S.Q. and A.P.; Validation, B.S.; Formal analysis, A.P.; Writing—original draft, A.A.; Writing—review & editing, A.P. and B.S.; Supervision, A.A. and B.S.; Project administration, A.A. and B.S. All authors have read and agreed to the published version of the manuscript.

Funding: This research received no external funding.

Data Availability Statement: Data available in a publicly accessible repository [20].

Conflicts of Interest: The authors declare no conflicts of interest.

References

1. Lu, L.; Han, X.; Li, J.; Hua, J.; Ouyang, M. A review on the key issues for lithium-ion battery management in electric vehicles. *J. Power Sources* **2013**, *226*, 272–288. [[CrossRef](#)]
2. Severson, M.H.; Attia, P.M.; Jin, N.; Perkins, N.; Jiang, B.; Yang, Z.; Chen, M.H.; Aykol, M.; Herring, P.K.; Fragedakis, D.; et al. Data-driven prediction of battery cycle life before capacity degradation. *Nat. Energy* **2019**, *4*, 383–391. [[CrossRef](#)]
3. Baghdadi, I.; Briat, O.; Deléatge, J.Y.; Gyan, P.; Vinassa, J.M. Lithium battery aging model based on Dakin’s degradation approach. *J. Power Sources* **2016**, *325*, 273–285. [[CrossRef](#)]
4. Zhang, D.; Dey, S.; Perez, H.; Moura, S. Remaining useful life estimation of Lithium-ion batteries based on thermal dynamics. In Proceedings of the 2017 American Control Conference (ACC), Seattle, WA, USA, 24–26 May 2017; pp. 4042–4047. [[CrossRef](#)]
5. Xu, X.; Tang, S.; Yu, C.; Xie, J.; Han, X.; Ouyang, M. Remaining Useful Life Prediction of Lithium-ion Batteries Based on Wiener Process Under Time-Varying Temperature Condition. *Reliab. Eng. Syst. Saf.* **2021**, *214*, 107675. [[CrossRef](#)]
6. Dong, Z.; Wei, J. A physics-based aging model for lithium-ion battery with coupled chemical/mechanical degradation mechanisms. *J. Electrochim. Acta* **2021**, *395*, 139133. [[CrossRef](#)]
7. Sun, Y.; Hao, X.; Pecht, M.G.; Zhou, Y. Remaining useful life prediction for lithium-ion batteries based on an integrated health indicator. *Microelectron. Reliab.* **2018**, *88–90*, 1189–1194. [[CrossRef](#)]
8. Lui, H.Y.; Li, M.; Downey, A.; Shen, S.; Venkat Nemani, P.; Ye, H.; VanElzen, C.; Jain, G.; Hu, S.; Laflamme, S.; et al. Physics-based prognostics of implantable-grade lithium-ion battery for remaining useful life prediction. *J. Power Sources* **2021**, *485*, 229327. [[CrossRef](#)]
9. Gou, B.; Xu, Y.; Feng, X. State-of-Health Estimation and Remaining-Useful-Life Prediction for Lithium-Ion Battery Using a Hybrid Data-Driven Method. *J. IEEE Trans. Veh. Technol.* **2020**, *69*, 10854–10867. Available online: <https://api.semanticscholar.org/CorpusID:226230557> (accessed on 11 October 2024). [[CrossRef](#)]
10. Harris, S.; O’Connor, P.; Cox, R.W. A time-domain approach for monitoring battery state of health (SOH) and remaining useful life (RUL). In Proceedings of the IECON 2014—40th Annual Conference of the IEEE Industrial Electronics Society, Dallas, TX, USA, 29 October–1 November 2014; pp. 3083–3087. Available online: <https://api.semanticscholar.org/CorpusID:3597355> (accessed on 11 October 2024).
11. Wei, J.; Dong, G.; Chen, Z. Remaining Useful Life Prediction and State of Health Diagnosis for Lithium-Ion Batteries Using Particle Filter and Support Vector Regression. *IEEE Trans. Ind. Electron.* **2018**, *65*, 5634–5643. [[CrossRef](#)]
12. Bak, T.; Lee, S. Accurate Estimation of Battery SOH and RUL Based on a Progressive LSTM with a Time Compensated Entropy Index. In Proceedings of the Annual Conference of the PHM Society, Scottsdale, AZ, USA, 24 September 2019.
13. Beganovic, N.; Söfftker, D. Remaining lifetime modeling using State-of-Health estimation. *Mech. Syst. Signal Process.* **2017**, *92*, 107–123. [[CrossRef](#)]
14. He, Y.J.; Shen, J.; Shen, J.F.; Ma, Z. State of health estimation of lithium-ion batteries: A multiscale Gaussian process regression modeling approach. *Aiche J.* **2015**, *61*, 1589–1600. [[CrossRef](#)]
15. Tang, R.; Zhang, P.; Ning, S.; Zhang, Y. Prediction of Battery SOH and RUL Based on Cooperative Characteristics in Voltage-Temperature-Time Dimensions. *J. Electrochem. Soc.* **2023**, *170*, 060535. [[CrossRef](#)]
16. Gupta, S.; Mishra, P. Estimation of SoC, SoH and RUL of Li-Ion Battery: A Review. In Proceedings of the 2023 5th International Conference on Energy, Power and Environment: Towards Flexible Green Energy Technologies (ICEPE), Shillong, India, 15–17 June 2023.
17. Zhang, D.; Baraldi, P.; Cadet, C.; Yousfi-Steiner, N.; Bérenguer, C.; Zio, E. An ensemble of models for integrating dependent sources of information for the prognosis of the remaining useful life of Proton Exchange Membrane Fuel Cells. *Mech. Syst. Signal Process.* **2019**, *124*, 479–501. [[CrossRef](#)]
18. Zhao, H.; Pan, D.; Chen, C. Intelligent Prognostics for Battery Health Monitoring Using the Mean Entropy and Relevance Vector Machine. *IEEE Trans. Syst. Man Cybern. Syst.* **2014**, *44*, 851–862.
19. Gurulakshmi, A.B.; Nijhawan, G.; Praveen; Tyagi, L.; Hussien, R. A review on Machine Learning Enhanced Predictive Maintenance for Electric Vehicle Power Electronics: A Pathway to Improved Reliability and Longevity. *E3S Web Conf.* **2024**, *505*, 03017.
20. Vilse, S.B.; Stroe, D.I. *Lithium-Ion Battery Degradation Dataset Based on a Realistic Forklift Operation Profile*; Mendeley Data; Aalborg University: Aalborg, Denmark, 2023. [[CrossRef](#)]
21. Jolliffe, I.T. *Principal Component Analysis*; Springer Series in Statistics; Springer: New York, NY, USA, 2002.
22. Pearson, K. On Lines and Planes of Closest Fit to Systems of Points in Space. *Philos. Mag.* **1901**, *2*, 559–572. [[CrossRef](#)]
23. Shiri, F.M.; Perumal, T.; Mustapha, N.; Mohamed, R. A Comprehensive Overview and Comparative Analysis on Deep Learning Models: CNN, RNN, LSTM, GRU. *arXiv* **2024**, arXiv:2305.17473.
24. Chauhan, N.S.; Kumar, N. Traffic Flow Forecasting Using Attention Enabled Bi-LSTM and GRU Hybrid Model. In *Neural Information Processing*; Tanveer, M., Agarwal, S., Ozawa, S., Ekbal, A., Eds.; Springer: Singapore, 2023; pp. 505–517.

25. Al Hamoud, A.; Hoenig, A.; Roy, K. Sentence subjectivity analysis of a political and ideological debate dataset using LSTM and BiLSTM with attention and GRU models. *J. King Saud Univ.-Comput. Inf. Sci.* **2022**, *34*, 7974–7987. [[CrossRef](#)]
26. Zulqarnain, M.; Ghazali, R.; Aamir, M.; Hassim, Y.M.M. An efficient two-state GRU based on feature attention mechanism for sentiment analysis. *Multimed. Tools Appl.* **2024**, *83*, 3085–3110. [[CrossRef](#)]

Disclaimer/Publisher’s Note: The statements, opinions and data contained in all publications are solely those of the individual author(s) and contributor(s) and not of MDPI and/or the editor(s). MDPI and/or the editor(s) disclaim responsibility for any injury to people or property resulting from any ideas, methods, instructions or products referred to in the content.